DOI: 10.1002/
Article type: Full Paper

Metal Soap Membranes for Gas Separation

*Qi Liu, Deepu J. Babu, Jian Hao, Mohammad Tohidi Vahdat, Davide Campi, Kumar Varoon Agrawal**

Dr. Q. Liu, Dr. D. J. Babu, J. Hao, M. T. Vahdat, Prof. K. V. Agrawal
Laboratory of Advanced Separations (LAS), École Polytechnique Fédérale de Lausanne (EPFL), Sion CH-1951, Switzerland.
E-mail: kumar.agrawal@epfl.ch

M. T. Vahdat, Dr. D. Campi
Theory and Simulation of Materials (THEOS) and National Centre for Computational Design and Discovery of Novel Materials (MARVEL), EPFL, Lausanne CH-1015, Switzerland.

Keywords: metal soaps, membranes, interfacial crystallization, melting, gas separation

Metal soaps or metal alkanoates are metal-organic complexes held together metal cations and the functional groups of hydrocarbon chains. They can be synthesized at a high yield by simply mixing the metal and organic sources, forming crystalline frameworks with diverse topology, and have been studied in the past because of their rich polymorphism like liquid crystals. Their ability to melt while retaining the crystalline properties upon cooling is unique among nanoporous materials and is especially attractive for membrane fabrication. Herein, we report metal-soaps as a new class of material for molecular separation. Three metal soaps, $Ca(SO_4C_{12}H_{25})_2$, $Zn(COOC_6H_{13})_2$, and $Cu(COOC_9H_{19})_2$ hosting lamellar structure with molecular-sized channels are synthesized. They are processed in thin, intergrown, polycrystalline films on porous substrates by two scalable methods, interfacial crystallization and melting with an extremely small processing time (a minute to an hour). The resulting crystalline films are oriented with the alkyl chains perpendicular to the porous substrate which favors molecular transport. The prepared membranes demonstrate attractive gas separation behavior, e.g., 200-nm-thick $Ca(SO_4C_{12}H_{25})_2$ membrane prepared in a minute using interfacial crystallization yielded H_2 permeance of 6.1×10^{-7} mol m^{-2} s^{-1} Pa^{-1} with H_2/CO_2 selectivity of 10.5.

1. Introduction

Molecular separation using membranes is highly energy-efficient because the driving force for separation does not rely on the relatively expensive thermal energy but on the chemical potential difference across the membranes.[1-9] Several materials and chemistries have been used to develop the selective layer of the membranes, including polymers,[2,7,10,11] carbon,[12-14] zeolites,[1,15,16] and more recently metal-organic frameworks (MOFs)[4,17-22] and covalent-organic frameworks (COFs).[23-27] One of the most sought-after strategies to develop the selective layer is to advance the material chemistry and engineering such that one can obtain a good separation performance (a combination of gas permeance and gas pair selectivity), while at the same time, can process the material in a scalable way. For example, polymers are predominately used as the selective material for membranes because they are highly processible. Rigid nanoporous materials with ordered pores such as zeolite, MOFs, and COFs have been successfully used to form the selective layer with improved performance, however, one compromises the processability. Typically, to obtain an attractive performance from these materials, one has to crystallize an intergrown polycrystalline film. However, to synthesize high-quality nanoporous membranes, generally, one needs to reduce the density of pinholes and grain-boundary defects which often require time-consuming complex steps. In this regard, the synthesis of gas-selective, nanoporous, crystalline materials that can be readily processed into high-quality thin films by scalable approaches is greatly desired.[28]

Metal soaps or metal alkanoates, well-known by their rich polymorphism and polymesomorphism, have been used as a barrier coating,[29-32,39,40] thermotropic ionic liquid crystals,[38] nonlinear-optical materials,[29] etc.[33-36] They are constructed by predominantly bonding between metal cations (Li^+, Na^+, K^+, Cs^+, Mg^{2+}, Ca^{2+}, Sr^{2+}, Ba^{2+}, Zn^{2+}, Cu^{2+}, Cd^{2+}, Co^{2+}, Ni^{2+}, Y^{3+}, Tb^{3+} etc.) and the functional head group (carboxylate (-COOH), sulfite (-SO_3H), sulfate (-SO_4H), etc.) of a hydrocarbon chain (alkyl, enyl, aryl, etc., with carbon

number > 3). The resulting M-O bonds are thermally and chemically robust making metal soaps attractive for practical applications. The MO_x polyhedra form a layer of rods/chains or sheets that are sandwiched between the layers of lipidic hydrocarbon chains, leading to a lamellar structure (**Figure 1** and **S1**). As early as the 1960's, Luzzati et al. reported the crystal structure of alkaline earth metal soaps by X-ray diffraction (XRD) where they revealed the ordered arrangements of metal cations and correlated the lattice parameters with the length of the hydrocarbon chain.[37]

Due to the high flexibility of the long alkyl chains in the structures, most metal soaps can melt at a moderate temperature (100-200 ˚C), forming a disordered/amorphous liquid phase or a mesophase, which was first discovered back in 1855.[38] The liquid phase can be readily cooling down, upon which, the disordered structure quickly turn back to the original crystalline state. Because of the hydrophobicity of the long alkyl chains, metal soaps have been used as a "green" corrosion barrier by constructing metal soaps on the surface of metals.[31] They also play an important role in analytical and preparative science as a means to reduce surface tension, for example, to unfold highly ordered macromolecules such as proteins.[39] Besides, due to the high polarization between metal cations and lipidic chains during melting, metal soaps have been proved to be attractive as a nonlinear-optical material.[31]

To the best of our knowledge, molecular separation using metal-soaps has not been reported. This presents an opportunity to evaluate this class of material for the preparation of gas separation membranes especially in the context of a large number of ordered porous metal soaps that could allow separation of several gas pairs. They are particularly attractive for membranes because the synthesis of metal soap is facile, and most of them crystallize rapidly in sufficiently high yields in aqueous solutions when the reactants (metal and organic sources) are mixed. Additionally, they provide processability advantage as one could synthesize the selective layer of a membrane (thin films) by exploiting the solid to liquid transition ability of

metal soaps and the fact that they do not lose crystallinity upon cooling down. Finally, the melting property could also be used in the post-synthetic healing of pinhole defects that often ruin the membrane selectivity, by simply annealing the film near the melting temperature.

Herein, three metal soaps, $Ca(SO_4C_{12}H_{25})_2$, $Zn(COOC_6H_{13})_2$ and $Cu(COOC_9H_{19})_2$, termed henceforth as CaC_{12}, ZnC_6, CuC_9, respectively, are synthesized in polycrystalline thin film morphology, loaded on porous supports, by two scalable methods: interfacial crystallization and melting. In the case of interfacial crystallization, a continuous film is formed on the surface of the water within one minute, following which the film could be easily transferred to porous substrates. In the case of the melting method, the membranes were formed by melting a layer of deposited metal-soap-crystals at 120 -150 ˚C in less than 1 hour. The resulting films are crystalline and are oriented on the porous support with the alkyl chains perpendicular to the substrates, favoring the molecular transport. Because of the large grain-size in these films (extending to several microns), all membranes show promising gas separation properties.

2. Results and Discussion

2.1. Crystal structure of metal soaps

Metal soaps are composed of two parts: a metal cation part and an organic part. The metal cations and the functional groups from the organic part form an inorganic backbone while the long alkyl chains attached to the backbone form a lamellar structure (**Figure 1** and **S1**). For example, CaC_{12} has a two-dimensional (2D) structure where the Ca^{2+} ions are bonded with the sulfate groups from sodium dodecyl sulfate (SDS) and form a 2D backbone, while dodecyl groups from SDS are located on both sides of the 2D layer (Figure 1A and 1B).[41] There are two distinct channels in CaC_{12}: one comprising of gaps between the dodecyl groups with the size of ca. 3.1 Å (the sizes were measured by calculating the shortest distances in the gap and subtracting the radii of the edge atoms), and the other inside the four-membered inorganic ring made of Ca^{2+}/sulfate groups with a size of ca. 0.5 Å (Figure 1B). The crystal structure of

ZnC_6 is similar to CaC_{12} (Figure 1C).[42] Zn^{2+} and carboxylate groups from heptanoic acid form a 2D backbone, with hexyl groups from heptanoic acid presenting in both sides of the layer, albeit with an asymmetric arrangement. The channel sizes between hexyl groups on the two sides of the 2D layer are ca. 3.2 and 3.3 Å (Figure 1D). The pore size of the four-membered ring made of Zn^{2+}/carboxylate groups is ca. 2.8 Å. In contrast, CuC_9 has a one-dimensional (1D) structure where a rod is formed by bonding of Cu^{2+} with the carboxylate groups of decanoic acid (Figure 1E), and nonadecyl groups extend away from the rod.[34] The channel formed between the gaps of the nonadecyl groups are ca. 2.9 Å in size (Figure 1F). The channel between Cu^{2+}/carboxylate rods is impermeable with a size of 1.5 Å.

2.2. Synthesis of metal soap membranes

CaC_{12} membranes were synthesized by the interfacial crystallization route (Figure 1G). During the synthesis of CaC_{12} powders, we noticed that a film was formed on the water surface spontaneously when the two reactants (SDS and calcium nitrate) were mixed (supplemental video and Figure 2A). This gave us a clue to synthesize CaC_{12} membranes by the interfacial crystallization route because one can prepare the membrane by simply lifting off the floating film. ZnC_6 and CuC_9 did not form a film at the air-water interface. Even when the surfactant chain-length was increased to up to 17 (e.g., CuC_{11}, CuC_{17}, Figure S7), we did not observe interfacial crystallization. Therefore, ZnC_6 and CuC_9 membranes were synthesized by the melting route attributing to the unique melting properties of these metal-soaps (Figure 1H).

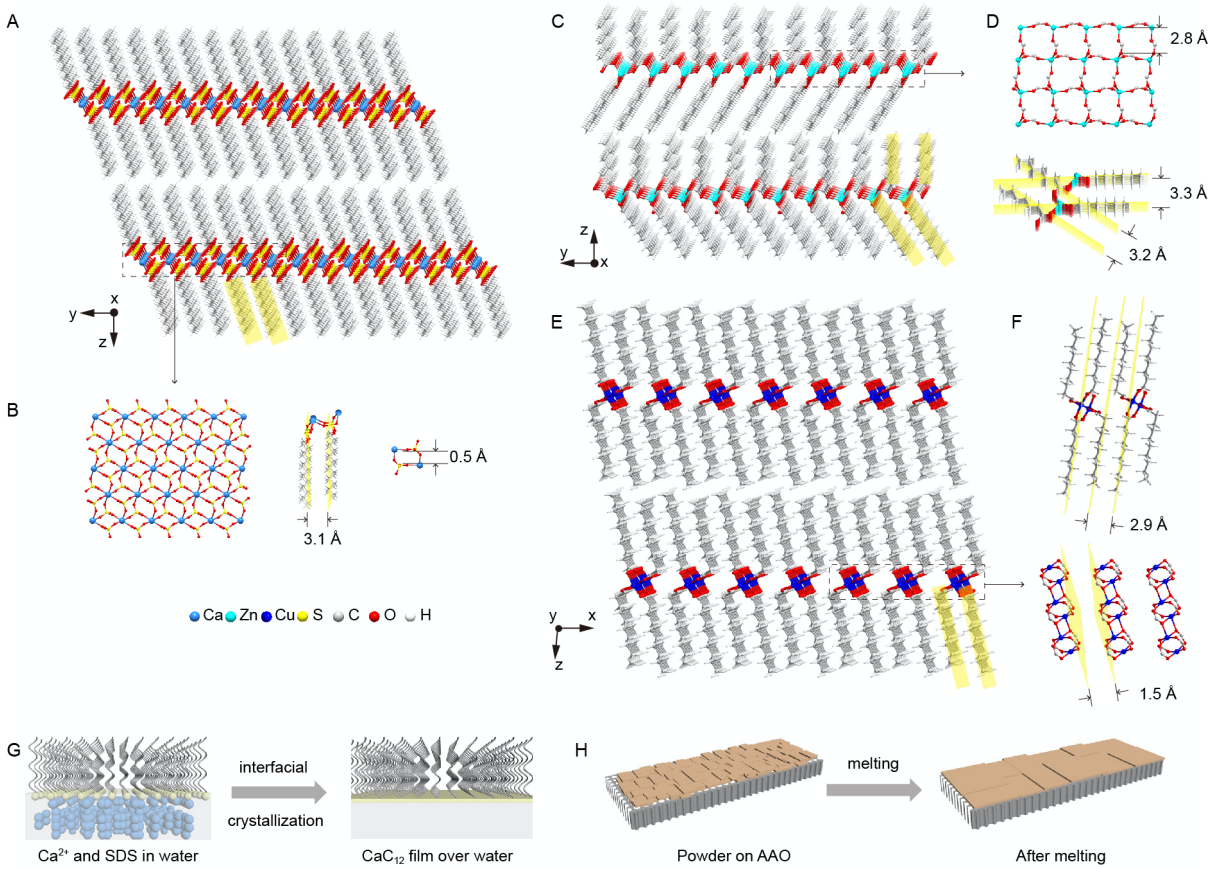

Figure 1. (A) Crystal structure of CaC_{12}. (B) Structure of the 2D layer and pore sizes in CaC_{12}. (C) Crystal structure of ZnC_6. (D) Structure of the 2D layer and pore sizes in ZnC_6. (E) Crystal structure of CuC_9. (F) Structure of the 1D rods and pore sizes in CuC_9. (G) Scheme of CaC_{12} membrane formed by interfacial crystallization. (H) Schematic of ZnC_6 and CuC_9 membranes formed by the melting.

For the synthesis of CaC_{12} membrane, SDS was added dropwise into the calcium nitrate aqueous solution (see methods). Because of its amphiphilic nature, SDS forms a film on the water surface. The sulfate groups of SDS reacted immediately with Ca^{2+} in the solution, forming a CaC_{12} film covering the whole water surface (Figure 2A and supplemental video). The defects in the floating film were quickly healed by the spontaneous reaction, and once the film formation was complete (usually in less than 1 minute), the final membrane was obtained by scooping the film with a porous substrate. Because of the flexibility of the process, we could use a number of porous supports such as porous polytetrafluoroethylene (PTFE), metal mesh, and anodic aluminum oxide (AAO).

For preparing ZnC_6 and CuC_9 membranes, we did not observe a similar film on the surface of the water. Therefore, we collected the precipitated metal soap crystals and prepared a suspension which was then vacuum filtered on to AAO substrates to form a deposit (Figure 1H, 3A, and 4A). Subsequently, the powder deposit was heated for a short time (120 ˚C and 40 min and 150 ˚C and 40 min for ZnC_6 and CuC_9, respectively) to obtain a melt. Finally, the molten film was cooled down to crystallize an intergrown membrane. Clogging of the AAO pores by the liquid melt was avoided to a large extent by flipping the AAO/powder assembly during heating (AAO at the top) exploiting the combined effect of the high viscosity of the liquid melt and gravity.

2.3 Characterizations of metal soap membranes

Upon optimization of the deposition steps, we could prepare crack-free membranes for all three metal soaps. CaC_{12} film prepared by the interfacial crystallization method led to an extremely thin membrane with a thickness of ca. 200 nm (Fig. 2A, 2B, and S3). The grains in the film were quite large exceeding several tens of microns. As a result, the film was quite smooth and lacked textural features when viewed by the scanning electron microscope (SEM) with high magnifications (Fig. 2A and S3). As for ZnC_6 and CuC_9, the melts generated by heating the powders to a temperature above their melting points filled up the void spaces resulting in a highly dense structure (Figure 3C, 3D, 4C, and 4D). The film thickness could be controlled by optimizing the vacuum filtration conditions. In the present case, the average film thicknesses are 2 and 4 μm for ZnC_6 and CuC_9 films, respectively. These thicknesses are much less than that from the powders deposited on AAO before melting (60 μm and 20 μm for ZnC_6 and CuC_9 powders, respectively). From the cross-section images, it is clear that the pore channels of AAO are not clogged by the metal soap. Therefore, we avoided a problem that has been previously reported with the melting route (Figure 3D and 4D).[43]

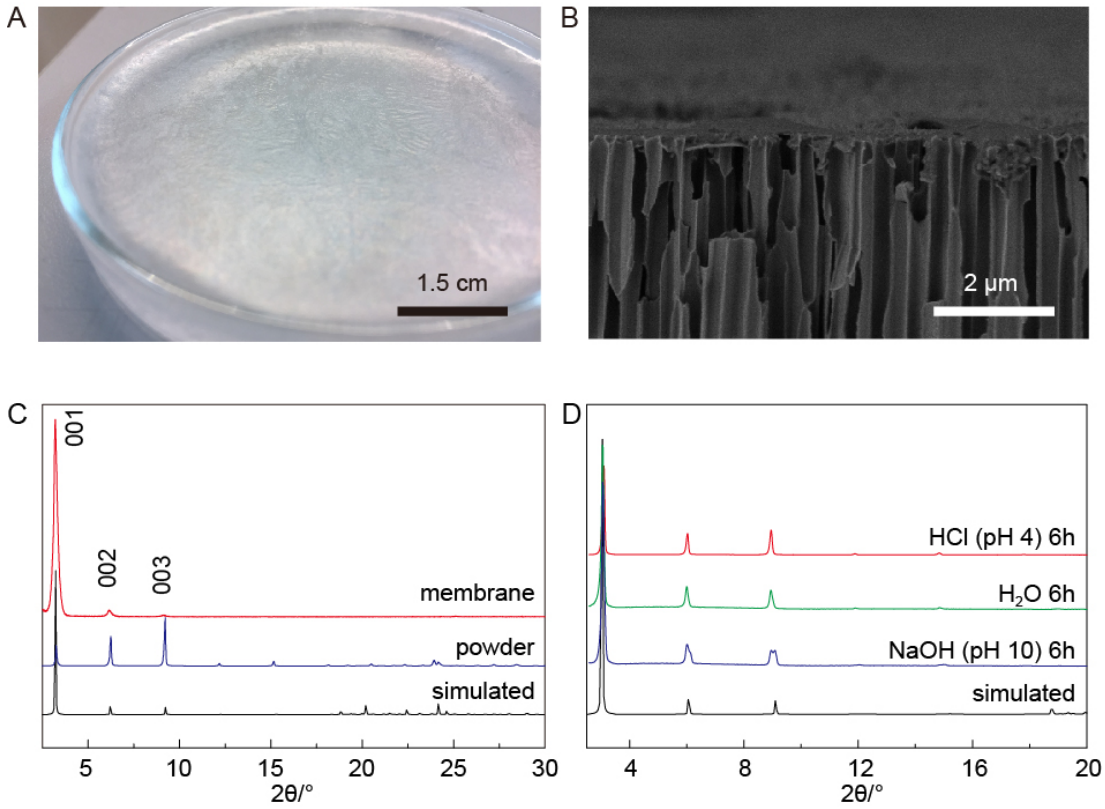

Figure 2. (A) Image of CaC_{12} film floating on water. (B) SEM cross-sectional view of CaC_{12} membrane on AAO with a pore size of 100 nm. (C) XRD of CaC_{12} powder and membrane on AAO with a pore size of 100 nm. (D) XRD of CaC_{12} powders after immersed in acidic and basic aqueous solutions for 6 h.

The crystallinity of the synthesized metal soap powders and the membranes was confirmed by XRD. The XRD patterns of three as-synthesized metal soap powders are almost identical to the simulated XRD patterns, indicating the phase purity of all three materials (Figure 2C, 3E, and 4E). Similarly, the XRD patterns showed high crystallinity for all three membranes (Figure 2C, 3E, and 4E). And the intensities of 00l peaks (001, 002 and 003 for CaC_{12}, 002, 004, and 006 for ZnC_6 and 001, 002, and 003 for CuC_9, respectively) from membranes were much higher compared to other peaks, which is in contrast to the simulated powder XRD patterns. This means the metal soap films are oriented on the substrate, with *c* axis perpendicular to the surface of the support. The stacking of layers is also evident in the cross-sectional SEM images of CaC_{12} and ZnC_6 (Figure 3D and S3). According to the crystal

structures of the three membranes (Figure 1 A, 1C, and 1E), it is clear that all the alkyl chains are in a similar direction of channels from the substrates, which could favor gas transport.

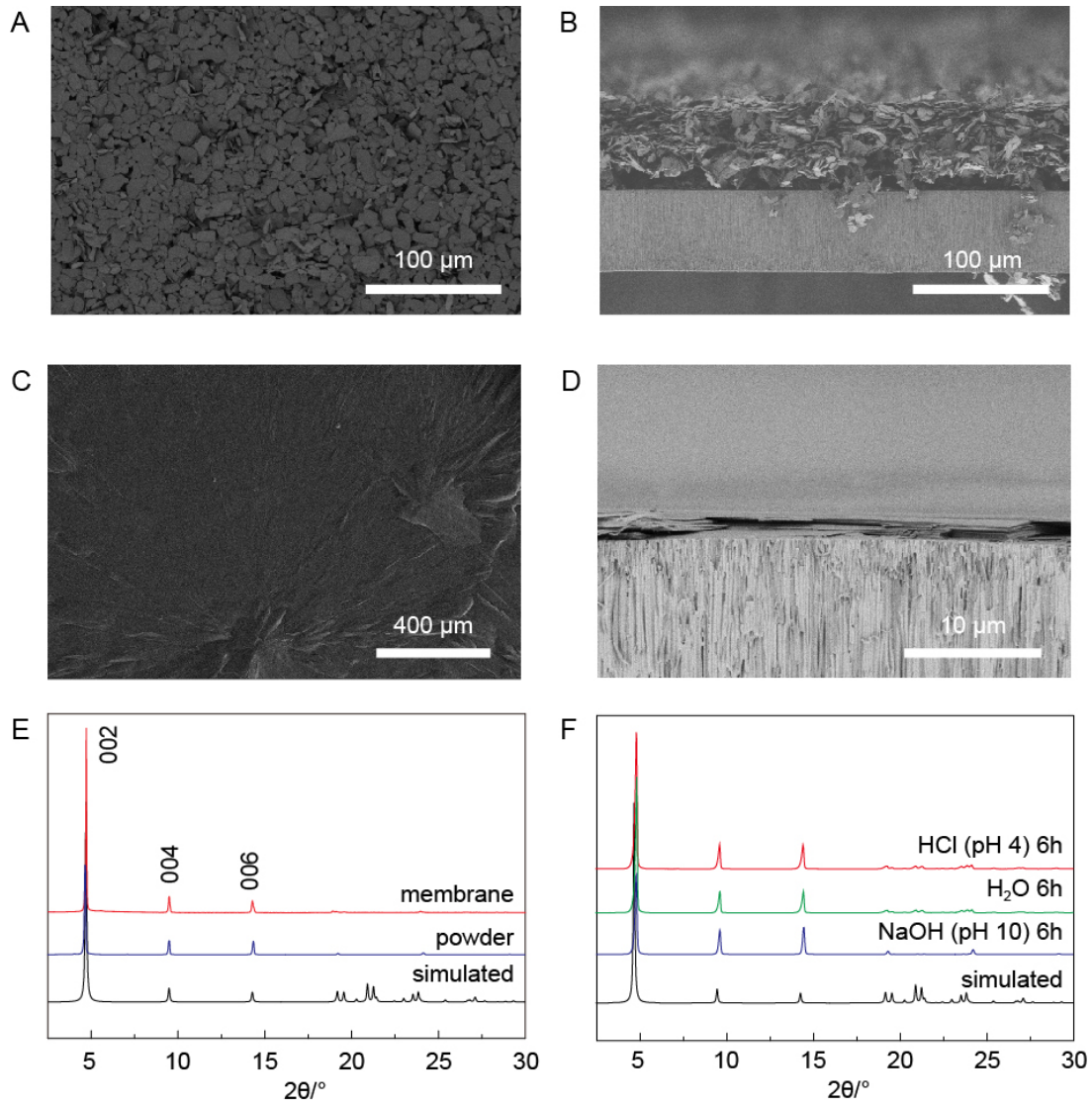

Figure 3. SEM images of the deposited ZnC_6 and as-synthesized membrane on AAO with a pore size of 100 nm, (A) and (C) top view, and (B) and (D) cross-sectional view, respectively. (E) XRD of ZnC_6 powder and membrane on AAO with a pore size of 100 nm. (F) XRD of ZnC_6 powders after immersed in acidic and basic aqueous solutions for 6 h.

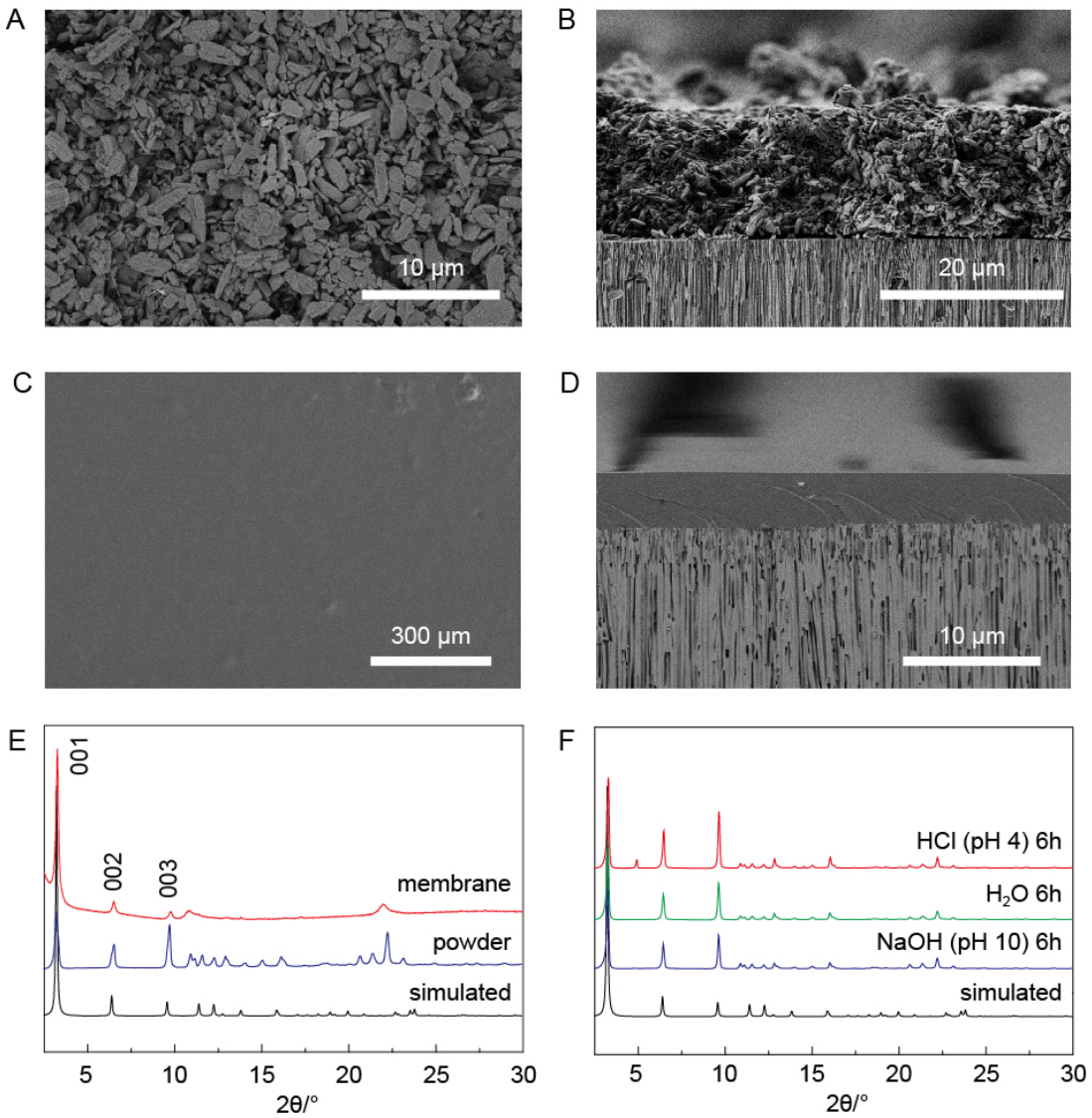

Figure 4. SEM images of the deposited CuC_9 and as-synthesized membrane on AAO with a pore size of 100 nm, (A) and (C) top view, and (B) and (D) cross-sectional view, respectively. (E) XRD of CuC_9 powder and membrane on AAO with a pore size of 100 nm. (F) XRD of CuC_9 powders after immersed in acidic and basic aqueous solutions for 6 h.

The thermal and chemical stability of the metal soap powders were also investigated. As shown in Figure 2D, 3F and 4F, after the powders of CaC_{12}, ZnC_6 and CuC_9 were immersed in water, HCl (pH = 4) and NaOH (pH = 10) aqueous solutions for 6 h, and XRD patterns were checked. CaC_{12} is stable in water and acid solutions. There are slight peaks splits around 6 and 9° of XRD after CaC_{12} in NaOH solution for 6 h, indicating partially unit-cell distortions could have happened (Figure 2D), however, this does not hinder the application of CaC_{12} in gas separation. ZnC_6 is stable in all solutions, and the XRD peaks maintained almost

the same as the simulated pattern (Figure 3F). For CuC_9, the powder survived in water and acid solutions for 6 h. A small new peak around 5˚ of CuC_9 powder in HCl solution appeared after 6 h, indicating the structure could start to change (Figure 4F). Although these three structures are similar, the different metals and organic parts lead to different behavior in acid and basic solutions. Thermogravimetric analysis (TGA) curves of CaC_{12}, ZnC_6, and CuC_9 in air atmosphere showed they were thermally stable up to 150 ˚C (Figure S2, S8, and S9), making them attractive for gas separation.

2.4 Gas permeation studies

Based on the crystal structure, the pore size relevant for the gas transport in the three metal soaps are ca. in the range of 2.8 - 3.3 Å. In addition, the flexibility of alkyl chains in the structures is expected to provide some tolerance for gas transport. All indicate that these structures could be useful in light gas separations such as hydrogen sieving (H_2, kinetic diameter of 2.89 Å) or carbon capture (CO_2, kinetic diameter of 3.3 Å). Accordingly, we tested the prepared crack-free membranes for gas separation.

The three metal soap films exhibited characteristically different permeation properties. The 200-nm-thick films of CaC_{12} prepared by interfacial crystallization exhibited the highest gas permeance among the studied metal-soap films (Figure 5A and 5B; data based on five membranes). Single component gas permeation studies at 25 ˚C revealed a H_2 permeance of 6.1×10^{-7} mol m^{-2} s^{-1} Pa^{-1} with an average H_2/N_2 and H_2/CH_4 selectivity of 4.4 and 5.5 respectively, which are higher than the corresponding Knudsen selectivities (3.7 and 2.8, respectively). However, CO_2 despite having a kinetic diameter of 3.3 Å, exhibited the lowest permeance resulting in H_2/CO_2 selectivity as high as 10.5. This anomalous behavior is likely due to much stronger adsorption of CO_2 with the CaC_{12} structure that may result from the strong bonding between Ca^{2+} and CO_2, where the bonding energy of Ca^{2+} and CO_2 is 8.0 kcal/mol, much larger than 4.6 kcal/mol for Ca^{2+} and N_2.[44] Similar behavior was also reported

for 2D ZIF-L films.[45] Considering the crystal structure of CaC_{12}, there are two kinds of pores with pore sizes 0.5 and 3.1 Å. Gas molecules cannot pass through the pores in the metal layers (0.5 Å) but they can transport across the gaps in the organic domain (3.1 Å). Because CaC_{12} membranes are oriented on the support, with the metal layers parallel to the surface of the support, gas molecules will inevitably pass the gaps between structure domains. This means Ca^{2+} ions on the edges of structural domains could attract CO_2, leading to the low CO_2 permeance in this membrane (Figure S10A).

Gas transport studies from ZnC_6 membranes revealed H_2/CO_2, H_2/CH_4, and He/CH_4 ideal selectivities of 6.2, 11.3, and 5.6, respectively, at 25 ˚C (Figure 5C and 5D; data based on three membranes). These selectivities are significantly higher than the corresponding Knudsen selectivities (4.7, 2.8, and 2.0, respectively), and indicate separation based on molecular size with permeance in the order of $H_2 > He > CO_2 > CH_4$, with average H_2 permeance of 2.1×10^{-9} mol m^{-2} s^{-1} Pa^{-1}. The lower permeance of He with respect to H_2, despite the smaller size of He, can be explained by negligible heat of adsorption of He. The relative permeation rates depending on the kinetic diameter of gases in ZnC_6 membranes indicate transport dominated by diffusion. This has origin in its structure. Both pore sizes of metal layers and organic layers (2.8, 3.2, and 3.3 Å) are suitable for the transition of gases (especially for H_2). In addition, organic chains in ZnC_6 is the shortest compared to CaC_{12} and CuC_9 (which means the structure of ZnC_6 could be more rigid than CaC_{12} and CuC_9). Gas molecules could pass both the metal layers (for H_2) and gaps between structure domains (Figure S10B).

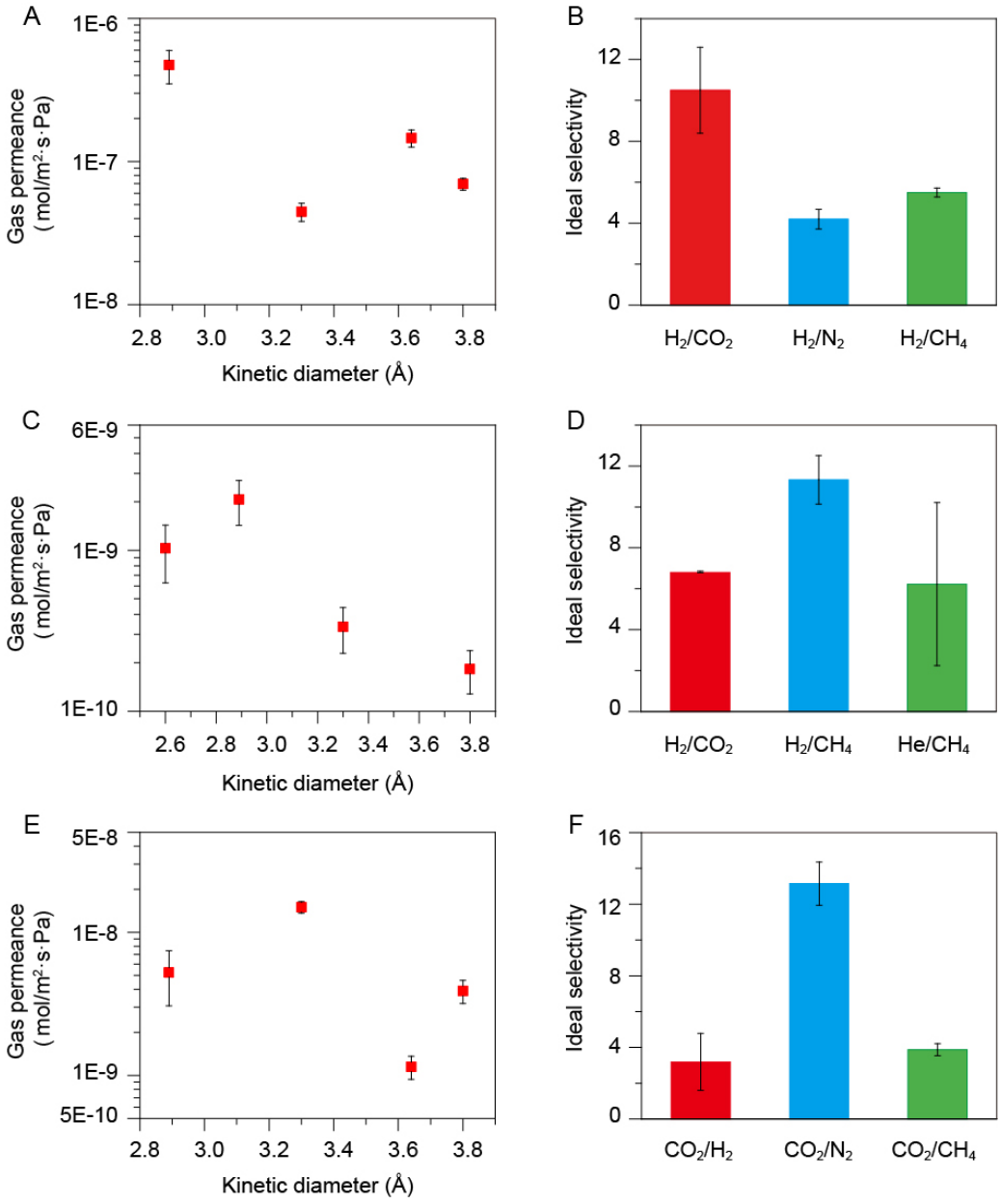

Figure 5. Gas permeances, (A) CaC_{12}, (C) ZnC_6 and (E) CuC_9, and ideal selectivities of membranes, (B) CaC_{12}, (D) ZnC_6 and (F) CuC_9, as a function of the kinetic diameters at 25 °C. Error bars in the figure represent the standard deviations across several membranes.

The permeation characteristic of CuC_9 was different from that of CaC_{12} and ZnC_6 membranes. With an average CO_2 permeance of 1.5×10^{-8} mol m^{-2} s^{-1} Pa^{-1}, CO_2 permeated faster than H_2 through the CuC_9 membrane. Similar to what is commonly observed with a number of nanoporous polymers (polymers with intrinsic microporosity or PIM, poly[1-(trimethylsilyl)-1-propyne or PTMSP, PDMS, etc.),[46-51] the single component gas permeance for CuC_9 decreased in the order $CO_2 > H_2 > CH_4 > N_2$ with CO_2/H_2, CO_2/CH_4 and CO_2/N_2

selectivities of 2.9, 3.9, and 13 respectively (Figure 5E and 5F, based on two membranes). The 1D rod like structures of CuC_9 are analogues to polymer chains which might explain the similar permeation characteristics.

In all, although these three materials are all metal soaps, their behaviors in gas permeations are different, attributing to their unique structure and chemical composition. ZnC_6 membranes appear to separate molecules based on their size, CuC_9 membranes act analogues to nanoporous polymers with a high permeation rate of CO_2, while CaC_{12} membranes inhibit the permeation rate of CO_2. The diverse gas separation performance indicates that metal soap membranes can act as flexible polymers as well as rigid nanoporous materials, attributing to their rich diversity of structures, which contain both long carbon chains and bonding of metal cations and functional groups, and are highly crystalline at the same time.

Compared to the recent reports of MOF glass membranes[43], metal soaps retain their crystallinity in the final membrane structure. It should be noted that the melting points of metal soaps are much lower than that of MOFs (about 100-200 ˚C versus 400 ˚C). The facile processability of the metal soap membranes prepared either by the simple interfacial crystallization technique or by the melting method and a large number of potentially interesting structures, make them an interesting class of materials for molecular separation.

3. Conclusion

In conclusion, we report for the first time, the synthesis of crack and defect-free metal soap membranes and their application in gas separation. The rapid interfacial crystallization and the melting methods demonstrated here adds to the ongoing efforts to rapidly synthesize crystalline nanoporous films to improve their scaleup potential. The diverse structure of metal-soaps is reflected in their gas separation behavior leading to performance resembling nanoporous materials as well as polymeric chains, attributing to the presence of inorganic

layers as well as organic channels in the metal soaps. There are many more possibilities of metal-soaps depending upon the combination of metal cation, surfactant chain length, and the functional group of the surfactant.

4. Experimental Section

The syntheses of metal soap powders were carried out by a slight adaptation of the method reported in the literature.[34,41,42] For CaC_{12}, 2.36 g $Ca(NO_3)_2 \cdot 4H_2O$ and 5.76 g SDS were dissolved in 10 ml deionized water, respectively. A white precipitate formed immediately after the two solutions were mixed. For ZnC_6, 2.97 g $Zn(NO_3)_2 \cdot 6H_2O$ was dissolved in 10 ml deionized water. A mixture of 2.60 g heptanoic acid and 0.8 g NaOH was also dissolved in 10 ml deionized water. The two solutions were then mixed, and a white precipitate appeared in few seconds. For CuC_9, 2.41 g $Cu(NO_3)_2 \cdot 3H_2O$ was dissolved in 10 ml deionized water. A mixture of 3.44 g decanoic acid and 0.8 g NaOH was also dissolved in 10 ml deionized water. Then the two solutions were mixed to get blue precipitate in a few seconds. In all cases, the precipitate was filtered and washed with water. The powder was obtained by drying in air overnight. For the synthesis of CaC_{12} membrane, 5 ml of 0.1 M of SDS was added dropwise into 10 ml of 0.1 M $Ca(NO_3)_2$ aqueous solution. Once the whole water surface was covered, the film was scooped using a suitable porous substrate. Several kinds of porous substrates were used including AAO hosting 100 and 20 nm pores, porous PTFE membranes with pore sizes of 300 nm and a metal mesh with pore sizes of 5 μm. All membranes were dried overnight under the ambient conditions. Both ZnC_6 and CuC_9 membranes were synthesized by the following recipe: At first, 10 mg of ZnC_6 or CuC_9 powders were dispersed in 20 ml deionized water by ultra-sonication for 30 mins. 2 ml of the suspension was subsequently vacuum filtered on AAO hosting 100 nm pores. Finally, the ZnC_6 or CuC_9 powder on AAO was heated at high temperatures for a fixed time (120 ˚C and 40 mins for ZnC_6 and 150 ˚C and 40 mins for CuC_9, respectively), and then cooled down slowly to form the membranes.

Supporting Information ((delete if not applicable))
Supporting Information is available from the Wiley Online Library or from the author.

Acknowledgements
We acknowledge our host institution, EPFL, for the generous support. This work was supported by European Research Council Starting Grant (805437-UltimateMembranes) and Swiss National Science Foundation Assistant Professor Energy Grant (PYAPP2_173645).

Received: ((will be filled in by the editorial staff))
Revised: ((will be filled in by the editorial staff))
Published online: ((will be filled in by the editorial staff))

References

[1]. N. Rangnekar, N. Mittal, B. Elyassi, J. Caro, M. Tsapatsis, *Chem. Soc. Rev.*, **2015**, *44*, 7128.

[2]. B. Seoane, J. Coronas, I. Gascon, M. Benavides, O. Karvan, Oğuz J. Caro, F. Kapteijn, J. Gascon, *Chem. Soc. Rev.*, 2015, **44**, 2421-2454.

[3]. F. Yang, F. Tao, C. Li, L. Gao, P. Yang, *Nature Commun.*, **2018**, *9*, 5443.

[4]. A. Huang, Q. Liu, N. Wang, Y. Zhu, J. Caro, *J. Am. Chem. Soc.*, **2014**, *136*, 14686.

[5]. H. Park, J. Kamcev, L. Robeson, M. Elimelech, B. Freeman, *Science* **2017**, *356*, 1138.

[6]. W. Koros, C. Zhang, *Nature Mater.*, **2017**, *16*, 289.

[7]. L. Wang, M. Boutilier, P. Kidambi, D. Jang, N. Hadjiconstantinou, R. Karnik, *Nature Nanotech.*, **2017**, *12*, 509.

[8]. H. Li, Z. Song, X. Zhang, Y. Huang, S. Li, Y. Mao, H. Ploehn, Y. Bao, M. Yu, *Science* **2013**, *342*, 95.

[9]. L. Prozorovska, Liudmyla, P. Kidambi, *Adv. Mater.*, **2018**, *30*, 1801179.

[10]. K. Xie, Q. Fu, C. Xu, H. Lu, Q. Zhao, R. Curtain, D. Gu, P. Webley, G. Qiao, *Energy Environ. Sci.*, **2018**, *11*, 544.

[11]. Z. Qiao, S. Zhao, M. Sheng, J. Wang, S. Wang, Z. Wang, C. Zhong, M. Guiver, *Nature Mater.*, **2019**, *18*, 163.

[12]. J. Wei, Y. Hu, Y. Liang, B. Kong, J. Zhang, J. Song, Q. Bao, G. Simon, S. Jiang, H. Wang, *Adv. Funct. Mater.*, **2015**, *25*, 5768.

[13]. F. Wang, P. Carbone, R. Joshi, R. Nair, A. Geim, A. H. Wu, Y. Su, I. Grigorieva, V. Kravets, *Science* **2014**, *343*, 752.

[14]. M. Pera-Titus, *Chem. Rev.*, **2014**, *114*, 1413.

[15]. K. Agrawal, B. Topuz, T. Pham, T. Nguyen, N. Sauer, N. Rangnekar, H. Zhang, K. Narasimharao, S. Basahel, L. Francis, C. Macosko, S. Al-Thabaiti, M. Tsapatsis, K. Yoon, *Adv. Mater.*, **2015**, *27*, 3243.

[16]. H. Zhang, Q. Xiao, X. Guo, N. Li, P. Kumar, N. Rangnekar, M. Jeon, S. Al-Thubaiti, K. Narasimha Rao, S. Basahel, B. Topuz, F. Onorato, C. Macosko, A. Mkhoyan, M. Tsapatsis, *Angew. Chem. Int. Ed.*, **2016**, *55*, 7184.

[17]. A. Brown, N. Brunelli, K. Eum, F. Rashidi, J. Johnson, W. Koros, C. Jones, S. Nair, *Science* **2014**, *345*, 72.

[18]. C. Kong, H. Du, L. Chen, B. Chen, *Energy Environ. Sci.*, **2017**, *10*, 1812.

[19]. G. He, M. Dakhchoune, J. Zhao, S. Huang, K. Agrawal, *Adv. Funct. Mater.*, **2018**, *28*, 170742.

[20]. D. Babu, G. He, J. Hao, M. Vahdat, P. Schouwink, M. Mensi, K. Agrawal, *Adv. Mater.*, **2019**, *31*, 1900855.

[21]. D. Babu, G. He, L. F. Villalobos, K. V. Agrawal, *ACS Sustainable Chem. Eng.*, **2019**, *7*, 49.

[22]. X. Ma, P. Kumar, N. Mittal, A. Khlyustova, P. Daoutidis, K. Mkhoyan, M. Tsapatsis, *Science* **2018**, *361*, 1008.

[23]. D. Shinde, G. Sheng, X. Li, M. Ostwal, A. Emwas,K. Huang, Z. Lai, *J. Am. Chem. Soc.*, **2018**, *140*, 14342.

[24]. S. Kandambeth B. Biswal, H. Chaudhari, K. Rout, H. Kunjattu, S. Mitra, S. Karak, A. Das, R. Mukherjee, U. Kharul, R. Banerjee, *Adv. Mater.*, **2017**, *29*, 1603945.

[25]. H. Fan, J. Gu, H. Meng, A. Knebel, J. Caro, *Angew. Chem. Int. Ed.*, **2018**, *57*, 4083.

[26]. C. Zhang, B. Wu, M. Ma, Z. Wang, Z. Xu. *Chem. Soc. Rev.*, **2019**, *48*, 3811.

[27]. H. Yang, L. Yang, H. Wang, Z. Xu, Y. Zhao, Y. Luo, N. Nasir, Y. Song, H. Wu, F. Pan, Z. Jiang, *Nature Commun.*, **2019**, *10*, 2101.

[28]. J. Hao, D. J. Babu, Q. Liu, H-Y. Chi, C. Lu, K. V. Agrawal, *J. Mater. Chem. A* **2020**, *8*, 7633.

[29]. G. Klimusheva, T. Mirnaya, Y. Garbovskiy, *Liq. Cryst. Rev.*, **2015**, *3*, 28.

[30]. R. Corbery, *Curr. Opin. Colloid In. Sci.*, **2008**, *13*, 288.

[31]. J. Peultier, E. Rocca, J. Steinmetz, *Corros. Sci.*, **2003**, *45*, 1703.

[32]. J. Peng, G. Barnes, I. Gentle, *Adv. Colloid Interface Sci.*, **2001**, *91*,163.

[33]. S. Tavares, F. Wypych, A. Letao, *Chem. Phys. Lett.*, **2015**, *636*, 154.

[34]. M. Riesco, F. Martinez-Casado, J. Cheda, I. Yelamos, I, Silva, T. Plivelic, S. Lopez-Andres, P. Ferloni, *Cryst. Growth Des.*, **2015**, *15*, 2005.

[35]. R. Miller, J. Cabral, E. Robles, N. Brookes, O. Ces, *CrystEngComm* **2018**, *20*, 6834.

[36]. A. Maneedaeng, A. Flood, B. Grady, K. Haller, *Cryst. Growth Des.*, **2011**, *11*, 2948.

[37]. V. Luzzati, A. Tardieu, T. Gulik-Krzywicki, E. Rivas, F. Reiss-Husson, *Nature* **1968**, *220*, 1351.

[38]. D. Blunk, K. Praefcke, V. Vill. *Handbook of Liquid Crystals*, Wiley-VCH'; **1998**.

[39]. A. Zapf, R. Beck, G. Platz, H. Hoffmann, *Adv. Colloid Interface Sci.*, **2003**, *100*, 349.

[40]. M. Zhou, P. R. Nemade, X. Lu, X. Zeng, E. S. Hatakeyama, R. D. Noble, D. L. Gin. *J. Am. Chem. Soc.,* **2007**, *129*, 9574.

[41]. G. Sakane, M. Tomohara, Y. Katayama, K. Hayashi, *Acta Cryst.*, **2010**. *E66*, 749.

[42]. F. Lacouture, J. Peultier, M. Francois, J. Steinmetz, *Acta Cryst.*, **2000**, *C56*, 556.

[43]. Y. Wang, H. Jin, Q. Ma, K. Mo, H. Mao, A. Feldhoff, X. Cao, Y. Li, F. Pan, Z. Jiang, *Angew. Chem. Int. Ed.*, **2020**, *59*, 4365.

[44]. R. G. Keesee, A. W. Castleman, *J. Chem. Phys. Ref. Data*, **1986**, *56*, 1011.

[45]. Z. Zhong, J. Yao, R. Chen, Z. Low, M. He, J. Z. Liu, H. Wang, *J. Mater. Chem. A* **2015**, *3*, 15715.

[46]. M. Carta, R. Malpass-Evans, M. Croad, Y. Rogan, J. C. Jansen, P. Bernardo, F. Bazzarelli, N. B. McKeown, *Science* **2013**, *339*, 303.

[47]. C. G. Bezzu, M. Carta, A. Tonkins, J. C. Jansen, P. Bernardo, F. Bazzarelli, N. B. McKeown, N. B. *Adv. Mater.* **2012**, *24*, 5930.

[48]. Q. Song, S. Cao, P. Zavala-Rivera, L. P. Lu, W. Li, Y. Ji, S. A. Al-Muhtaseb, A. K. Cheetham, E. Sivaniah, *Nature Commun.*, **2013**, *4*, 1918.

[49]. M. Carta, M. Croad, R. Malpass-Evans, J. C. Jansen, P. Bernardo, G. Clarizia, K. Friess, M. Lanc, N. B. McKeown, *Adv. Mater.* **2014**, *26*, 3526.

[50]. Ai, M., Shishatskiy, S., Wind, J., Zhang, X., Nottbohm, C. T., Mellech, N., A. Winter, H. Vieker, J. Qiu, K. J. Dietz, A. Gölzhäuser, A. Beyer, *Adv. Mater.* **2014**, *26*, 3421.

[51]. S. Li, Z. Wang, X. Yu, J. Wang, S. Wang, *Adv. Mater.* **2012**, *24*, 3196.

The table of contents entry should be 50–60 words long, and the first phrase should be bold.

Three highly crystalline metal soap membranes, $Ca(SO_4C_{12}H_{25})_2$, $Zn(COOC_6H_{13})_2$, and $Cu(COOC_9H_{19})_2$, are synthesized by scalable techniques namely, interfacial crystallization and melting, with the processing time of a minute to an hour. The molecular-sized channels (2.8 - 3.3 Å) of these metal soaps led to the realization of attractive gas separation performances.

Keyword

metal soaps, membranes, interfacial crystallization, melting, gas separation

Qi Liu, Deepu J. Babu, Jian Hao, Mohammad Tohidi Vahdat, Davide Campi, Kumar Varoon Agrawal*

Title ((no stars))

Metal Soap Membranes for Gas Separation

ToC figure ((Please choose one size: 55 mm broad × 50 mm high **or** 110 mm broad × 20 mm high. Please do not use any other dimensions))

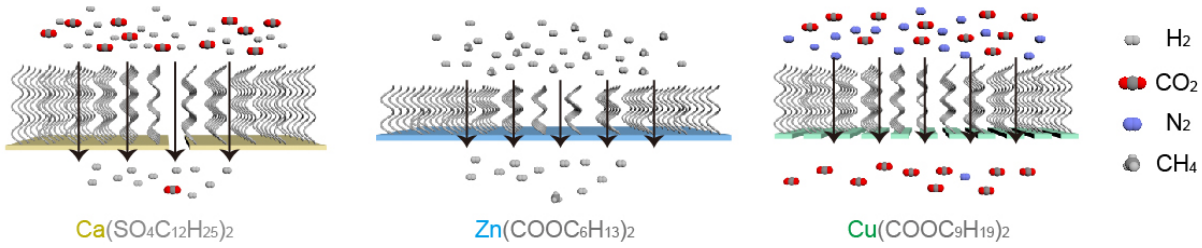

TOC

((Supporting Information can be included here using this template))

Supporting Information

Metal Soap Membranes for Gas Separation

*Qi Liu, Deepu J. Babu, Jian Hao, Mohammad Tohidi Vahdat, Davide Campi, Kumar Varoon Agrawal**

Chemicals and Instruments

Calcium nitrate tetrahydrate ($Ca(NO_3)_2{\cdot}4H_2O$), sodium dodecyl sulfate (SDS), copper nitrate trihydrate ($Cu(NO_3)_2{\cdot}3H_2O$), zinc chloride hexahydrate ($Zn(NO_3)_2{\cdot}6H_2O$), heptanoic acid, sodium hydroxide (NaOH), decanoic acid were purchased from Alfa Aesar. All chemicals were used without further purifications.

SEM measurements were performed on Teneo scanning electron microscope operating at 1 kV. PXRD data were measured at a Bruker D8 Discover diffractometer with a Lynxeye XE detector, operated at 40 kV, 400 mA for Cu Kα (λ = 1.5406 Å) at ambient temperature and pressure. TGA data were recorded on a PerkinElmer TGA 800 in the air with a heating rate of 10 °C/min.

The gas separation performance of all membranes was recorded on a homemade permeation setup described in detail in a previous publication[1]. The absolute pressure difference between the feed side and the permeate side of the membrane, for some measurements, was 0 bar for CaC_{12} membranes and was 0.5 bar for ZnC_6 and CuC_9 membranes. The pressure on the feed was maintained at 1-2 bar and on the permeate side at 1 bar during the measurements. All measurements were done after reaching the steady-state with argon as the sweep gas. The membranes were sealed with epoxy on a stainless-steel annular disk. The composition of the permeate was analyzed using an online Hiden Analytical HPR-20 mass spectrometer. The membrane cell along with the feed and sweep gas lines were heated inside a convection oven to control the temperature of the measurement. The permeances, Ji, of gas i was calculated by Eq. S1

$$Ji = Xi/(A{\cdot}\Delta Pi) \qquad \text{(S1)}$$

where *Xi* is the molar flow rate of component *i* across the membrane area (A) and ΔPi is the transmembrane pressure difference for the component *i*. The ideal selectivity α_{ij} of two gases (*i* and *j*, where *i* is the faster permeating gas) was calculated by Eq. S2

$$\alpha_{ij} = Ji/Jj \quad \text{(S2)}$$

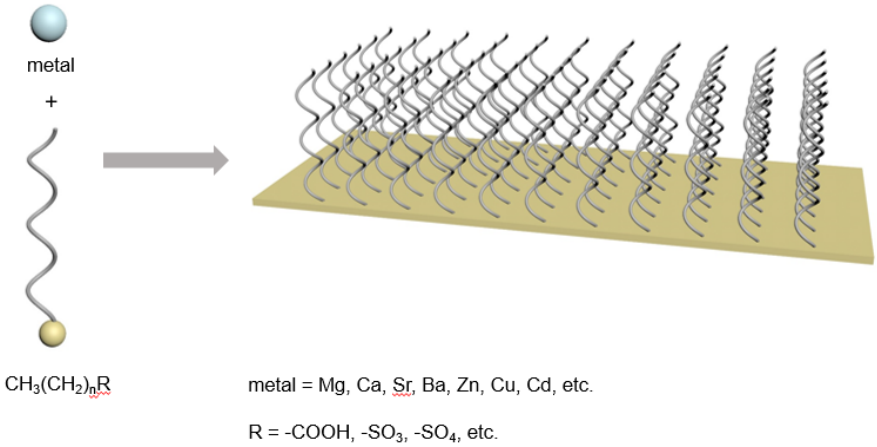

Figure S1. Scheme of structures of some metal soaps. One side of carbon chains is showed here for clarity.

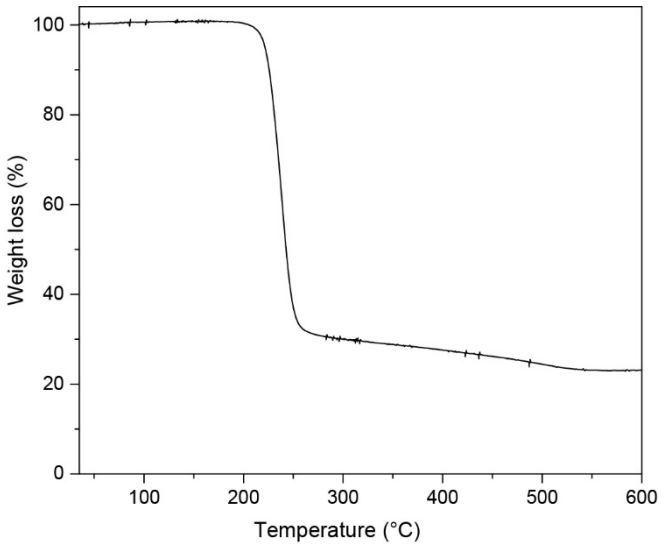

Figure S2. TGA curve of CaC_{12}.

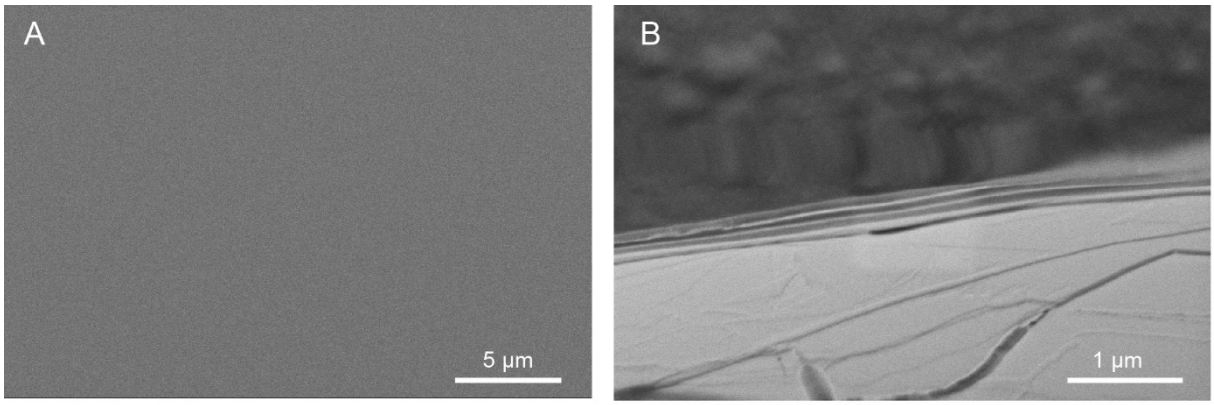

Figure S3. SEM image of CaC_{12} membrane on Si wafer. The cracks in panel (B) is the cross-section of this membrane, which clearly show the layers of CaC_{12}.

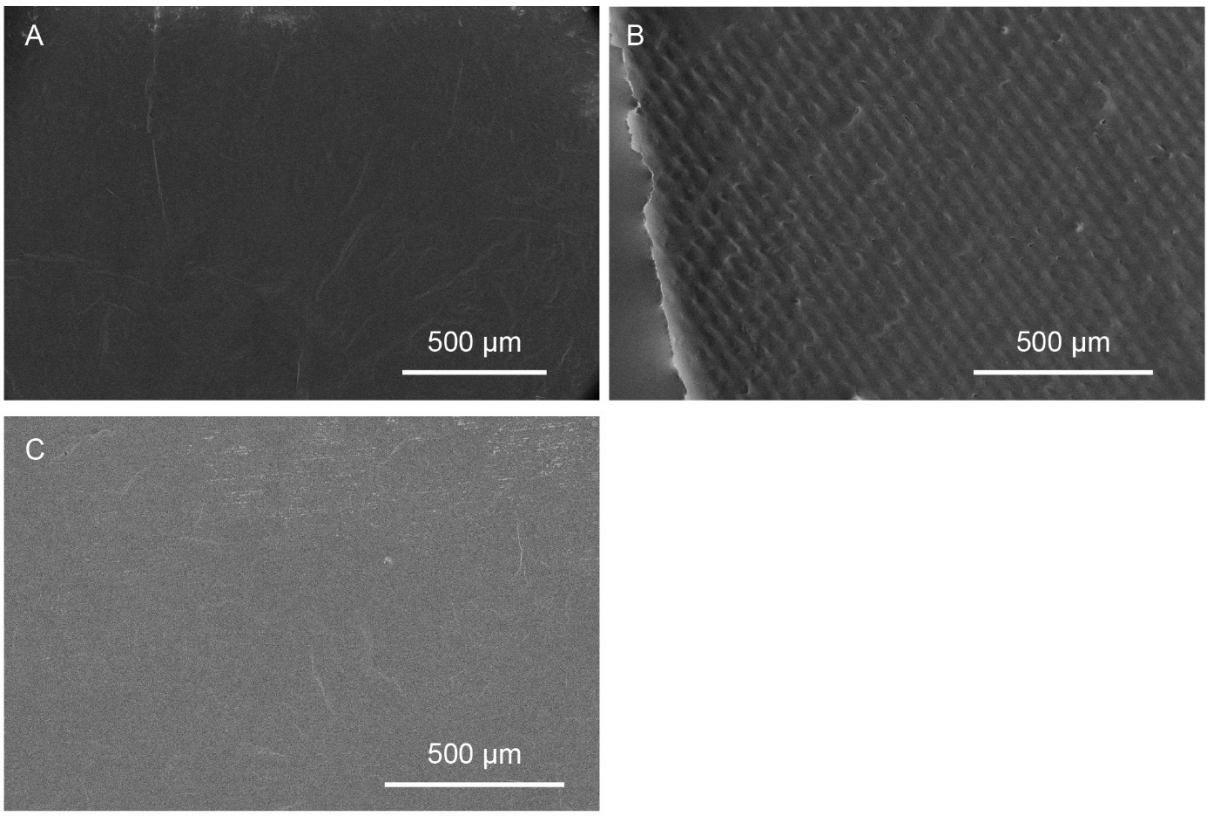

Figure S4. SEM images of CaC_{12} membrane on PTFE (A), metal mesh (B), and AAO with a pore size of 20 nm (C).

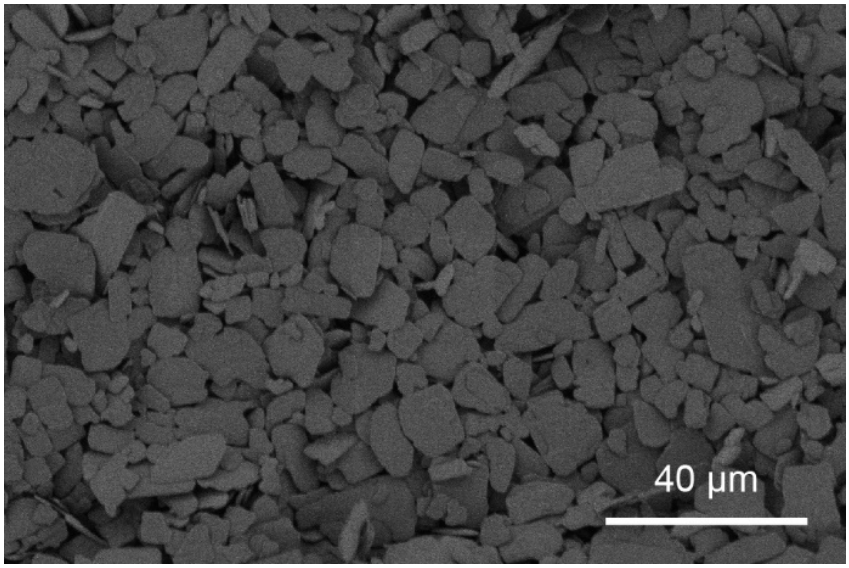

Figure S5. SEM images of ZnC_6 powders.

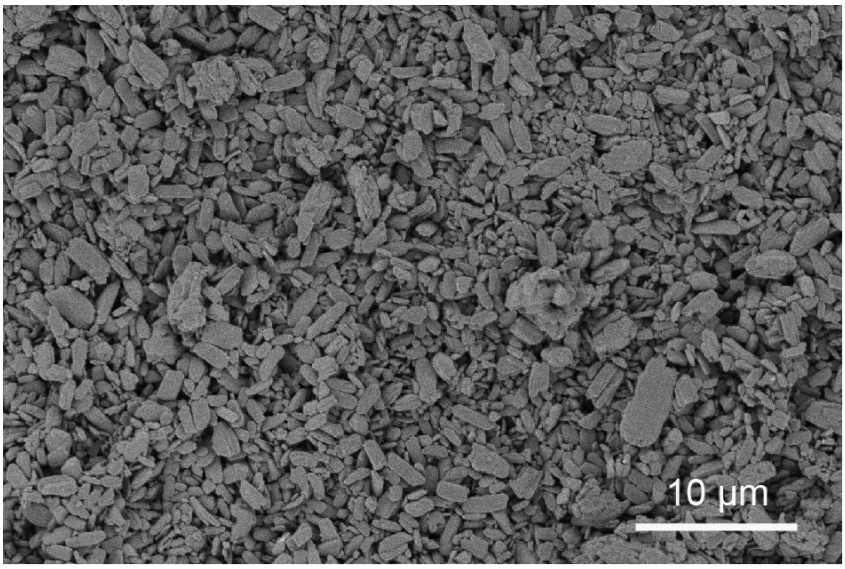

Figure S6. SEM images of CuC_9 powders.

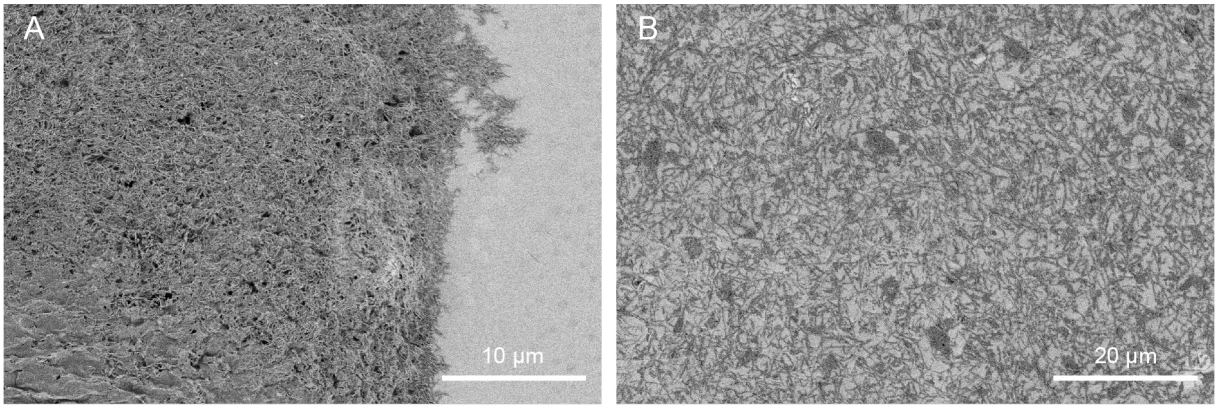

Figure S7. SEM images of CuC_{11} ($Cu(COOC_{11}H_{23})_2$) (A) and CuC_{17} ($Cu(COOC_{17}H_{35})_2$) (B).

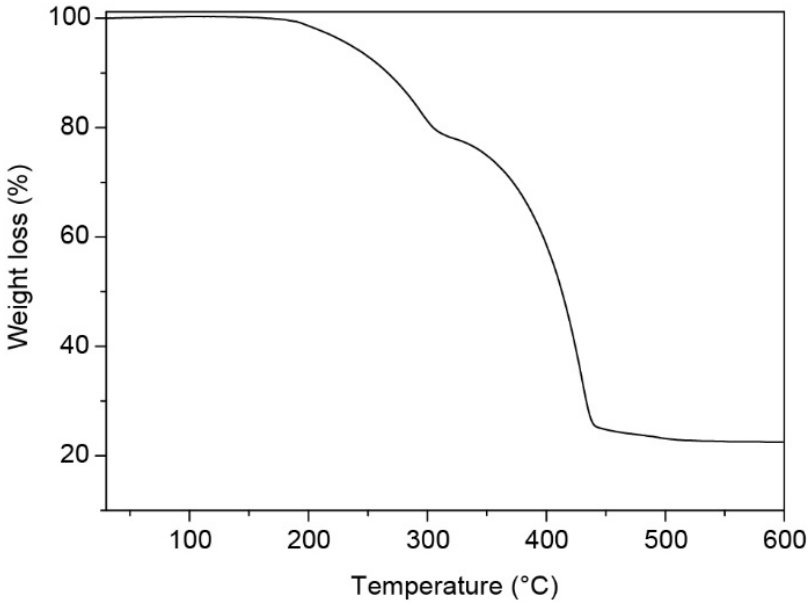

Figure S8. TGA curve of ZnC_6.

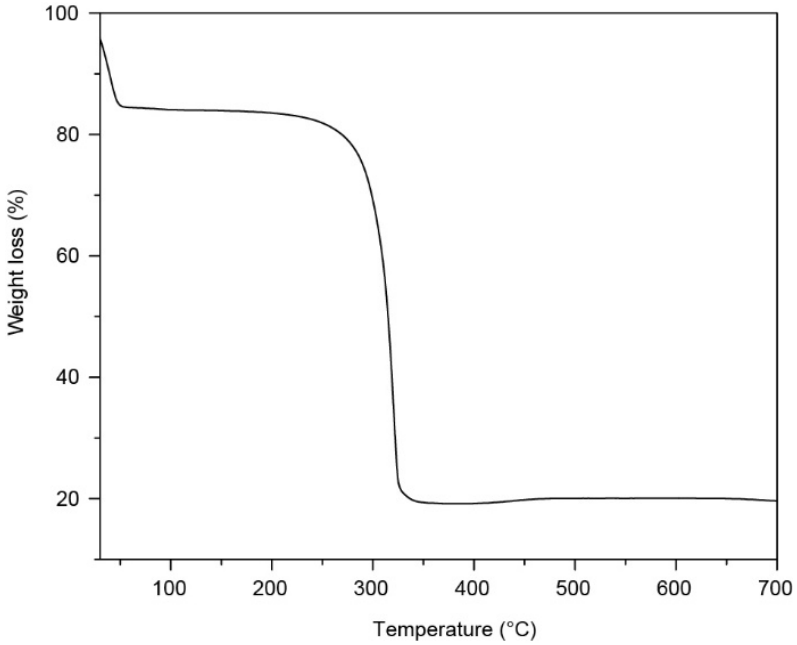

Figure S9. TGA curve of CuC_9. The initial weight loss before 100˚C could due to the loss of water.

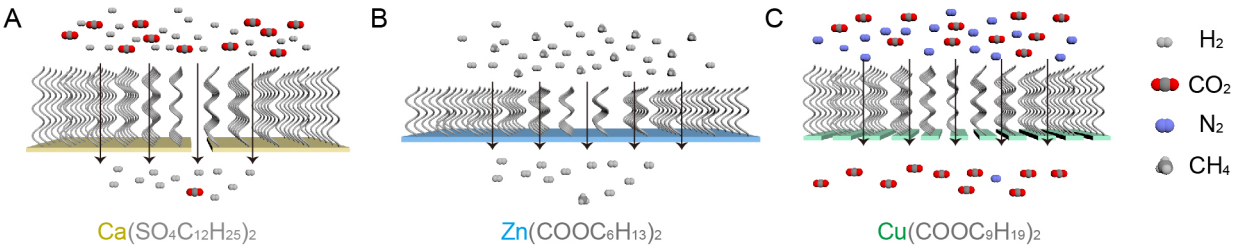

Figure S10. Scheme of transitions of gases through membranes. (A) CaC_{12}, (B) ZnC_6 and (C) CuC_9.

Reference

1. G. He, M. Dakhchoune, J. Zhao, S. Huang, K. V. Agrawal, *Adv. Funct. Mater.* **2018**, *28*, 1707427.